Noradrenaline-Functionalized Hyperbranched Fluoropolymer-Poly(ethylene glycol) Cross-Linked Networks As Dual-Mode, Anti-Biofouling Coatings

ARTICLE *in* ACS NANO · FEBRUARY 2012

Impact Factor: 12.88 · DOI: 10.1021/nn204431m · Source: PubMed

8 AUTHORS, INCLUDING:

Daniel Rittschof
Duke University
219 PUBLICATIONS **6,460** CITATIONS
SEE PROFILE

Andrew Mount
Clemson University
54 PUBLICATIONS **1,588** CITATIONS
SEE PROFILE

Karen L Wooley
Texas A&M University
328 PUBLICATIONS **17,492** CITATIONS
SEE PROFILE

Noradrenaline-Functionalized Hyperbranched Fluoropolymer–Poly(ethylene glycol) Cross-Linked Networks As Dual-Mode, Anti-Biofouling Coatings

Philip M. Imbesi,[†,‡,∥] Neeraj V. Gohad,[§,∥] Michael J. Eller,[†] Beatriz Orihuela,[⊥] Dan Rittschof,[⊥] Emile A. Schweikert,[†,*] Andrew S. Mount,[§,*] and Karen L Wooley[†,‡,*]

[†]Department of Chemistry, Texas A&M University, College Station, Texas 77842, United States, [‡]Department Chemical Engineering, Texas A&M University, College Station, Texas 77842, United States, [§]Department of Biological Sciences, Clemson University, Clemson, South Carolina 29634, United States, and [⊥]Zoology Department and School of the Environment, Duke University Marine Laboratory, Beaufort, North Carolina 28516, United States. [∥]These authors contributed equally.

ABSTRACT The strategy of decorating anti-biofouling hyperbranched fluoropolymer–poly-(ethylene glycol) (HBFP-PEG) networks with a settlement sensory deterrent, noradrenaline (NA), and the results of biofouling assays are presented. This example of a dual-mode surface, which combines both passive and active modes of antibiofouling, works in synergy to improve the overall antibiofouling efficiency against barnacle cyprids. The HBFP-PEG polymer surface, prior to modification with NA, was analyzed by atomic force microscopy, and a significant distribution of topographical features was observed, with a nanoscopic roughness measurement of 110 ± 8 nm. NA attachment to the surface was probed by secondary ion mass spectrometry to quantify the extent of polymer chain-end substitution with NA, where a 3- to 4-fold increase in intensity for a fragment ion associated with NA was observed and 39% of the available sites for attachment were substituted. Cytoskeletal assays confirmed the activity of tethered NA on adhering oyster hemocytes. Settlement assays showed deterrence toward barnacle cyprid settlement, while not compromising the passive biofouling resistance of the surface. This robust strategy demonstrates a methodology for the incorporation of actively antibiofouling moieties onto a passively antibiofouling network.

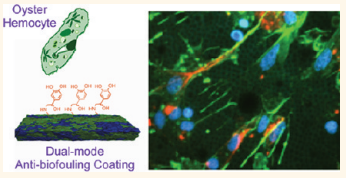

KEYWORDS: antibiofouling · noradrenaline · fluoropolymers · coating · amphiphilic · fouling deterrence

There are significant efforts underway worldwide to produce coatings that can be applied in the marine environment, for instance, to address the issue of biofouling on ship hulls, which can result in up to 70% increased fuel consumption and added operational costs.[1,2] Barnacle growth alone can reach 150 kg/m^2 in just 6 months.[3] Marine biofouling has been controlled, traditionally, through the use of antibiofouling paints that rely on the release of toxic agents,[4] such as organotin compounds, which are banned from use, and copper ablatives, the usage of which is being restricted, with a USA-wide regulatory decision expected in *ca*. 2015.[5,6] Action had been taken to ban the use of organotin paints because of the irreversible accumulation of the leachates in the sediment that results in unwanted environmental effects; similar environmental accumulation of copper in seawater, estimated to be 15 × 10^6 kg/yr worldwide, is becoming increasingly problematic.[7] Next-generation materials that are environmentally benign are desired.[8] Leading commercially available formulations often incorporate low surface energy polymer components, *e.g.*, silicones (Intersleek700, SeaGuard, *etc.*) and/or fluoropolymers (Intersleek900, *etc.*), to inhibit initial adhesion of biofouling organisms and promote their release,[9] each by passive modes of action. Antibiofouling coatings that present tethered biocidal groups, for example, quaternary ammonium salts,[10] and commercially available formulations that leach biocides (Irgarol, ZPT, Diuron, Sea-Nine)[7] operate by active modes of antibiofouling. It was hypothesized that the combination of these two distinctive modes of action would lead to superior antibiofouling coatings. As our interests are in the development of nontoxic antibiofouling coatings, we chose to avoid the use of biocidal agents and instead designed a multifunctional polymer coating that presents bioactive fouling-deterrent molecules[11] across a nanoscopically complex surface that provides for additional passive antibiofouling.

* Address correspondence to schweikert@mail.chem.tamu.edu; mount@clemson.edu; wooley@mail.chem.tamu.edu.

Received for review November 15, 2011 and accepted January 18, 2012.

Published online January 25, 2012
10.1021/nn204431m

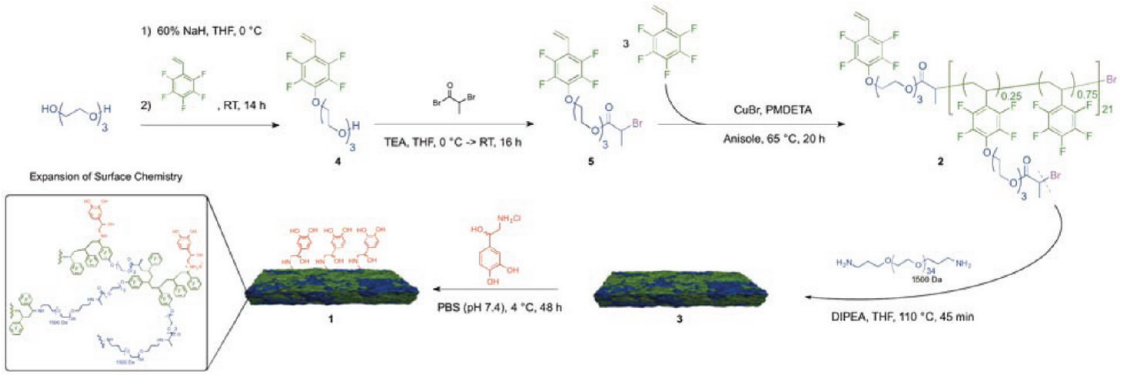

Scheme 1. Synthesis of noradrenaline-functionalized HBFP-PEG thin films (NA-HBFP-PEG), 1.

Previous studies by our laboratory investigating antibiofouling coatings comprised of hyperbranched fluoropolymers (HBFP) cross-linked with poly(ethylene glycol)s (HBFP-PEG)[12] have led to optimization of the chemistries and mechanical properties.[13,14] Fluoropolymers were chosen because of their low surface energy and extensive use in marine applications,[15−17] and PEGs were incorporated into the system because of their demonstrated resistance to protein adsorption.[18−20] The HBFP-PEG passive mode of antibiofouling is thought to be generated from a combination of complex surface topographies, morphologies, and compositions over nano- and microscopic dimensions,[21−23] inhibiting protein adhesion and whole organism settlement simultaneously.

The possibility of using soluble noradrenaline (NA), an adrenoreceptor agonist that is known to inhibit larval settlement in oysters[24−26] and barnacles,[27,28] as an antibiofouling agent has been explored previously, without NA being covalently bonded to the substrates.[29] Therefore, NA is an attractive moiety for tethering into environmentally benign, passively antibiofouling coatings to add the active mode of action, directly at the surface. Previous studies by Gohad *et al.* probed the interactions between NA tethered to poly(methacrylic acid) (PMAA) and poly(2-hydroxyethyl acrylate) (PHEMA) brushes and hemocytes of the Eastern Oyster, *Crassostrea virginica*.[11] These studies showed that NA molecules covalently linked to polymer brushes retained their bioactivity and were able to induce physiological changes in the hemocytes. Settlement assays using barnacle cyprids identified that the concentration of NA on the surface was sufficient to preserve the ability of NA-conjugated polymers to deter larval settlement. Questions remained, however, as to what extent the NA was covalently bound to the surface and whether advanced antibiofouling polymer substrates would provide enhanced performance.

In this work, NA was incorporated into HBFP-PEG to produce a highly complex, dual-mode antibiofouling polymer coating, with confirmation of its surface presentation and biological activity. This system utilized a new generation of HBFP bearing ethylene glycol units,[30] which was cross-linked with PEG. After deposition and curing, the passive mode of antibiofouling was provided by the complex surface topography and chemical heterogeneity. The coating surface properties were characterized by atomic force microscopy and contact angle experiments. Bromoacetyl and bromobenzyl functionalities at the HBFP chain ends, unconsumed during cross-linking, allowed for surface modification reactions with NA. Decoration of the HBFP-PEG with this small molecule provided the active mode of fouling deterrence. The extent of substitution was monitored *via* secondary ion mass spectrometry (SIMS), a versatile technique capable of analyzing a wide range of materials, including polymers, semiconductor assemblies, metals, biological samples, and nano-objects.[31−34] The technique employs a primary ion that impinges on a surface, resulting in the emission of secondary ions, electrons, and neutral species.[35] Cluster SIMS exhibits emission from the top 5 to 10 nm of a surface, allowing for the analysis of only the top fraction of a material. Therefore, NA that is sequestered into the bulk of the material, in this study, would not contribute to the mass spectrum obtained. Understanding the surface chemistry and the extent to which the substrate is decorated with this active deterrent allowed for correlation of the surface coverage to biofouling performance. Additionally, a comprehensive characterization study was performed against oyster hemocytes and barnacle cyprids on both unmodified HBFP-PEG and modified NA-HBFP-PEG surfaces to assess the enhanced organismal response to the dual-mode surface.

RESULTS AND DISCUSSION

The dual-mode, antibiofouling surface, **1** (Scheme 1), was designed to combine amphiphilic, morphologic, and topographic complexities of HBFP-PEG with the active deterrence of NA. The synthetic approach, therefore, relied upon reactive bromoacetyl and bromobenzyl functionalities at the chain ends of HBFP, **2**, to undergo the cross-linking reactions with diamino-terminated PEG, affording **3**, and also the chemical

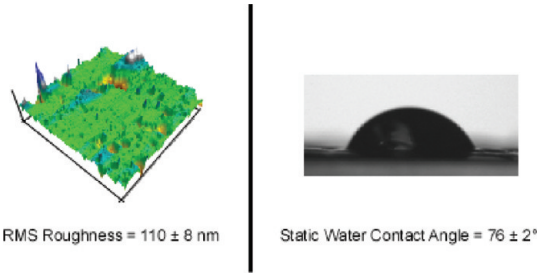

Figure 1. Atomic force microscopy (AFM) of HBFP-PEG films, 3 (left), and static water contact angle (right) after swelling in water overnight. AFM → scan size = 50 × 50 μm^2; *z*-axis = 1.0 μm.

modification reactions with NA to give **1**. The particular HBFP utilized, **2**, was of a unique chemical composition and structure, by linking hydrophobic and hydrophilic characteristics on a molecular level throughout the hyperbranched polymer framework.[30] The HBFP was synthesized *via* atom transfer radical self-condensing vinyl copolymerization (ATR-SCVCP) to control the molecular weight of the polymer and yield the reactive chain ends. The preparation of **2**, therefore, began from the nucleophilic aromatic substitution of the *para*-fluorine of 2,3,4,5,6-pentafluorostyrene (PFS) with an excess of tri(ethylene glycol) (TrEG), to give **4**, followed by esterification with 2-bromoisopropionyl bromide to yield the amphiphilic initiating monomer (inimer) **5** for ATR-SCVCP. Copolymerization of **5** with three molar equivalents of PFS achieved **2**, bearing TrEG throughout the backbone of the polymer.[12,30] A robust free-standing thin film, **3**, was then obtained from deposition and curing of **2** with a diamino-poly(ethylene glycol) (DA-PEG) in the presence of base. Incubating the cross-linked networks in water leached residual organic compounds and also released **3** from the substrate. Films of **3** were incubated in a PBS buffer solution of noradrenaline at 4 °C in the dark, to allow for substitution of the alkyl bromide functional handles on the surface to yield the noradrenaline-modified HBFP-PEG film, **1** (NA-HBFP-PEG). A series of replicates, **1a**–**d** and **3a**–**d**, was prepared to allow for complete physicochemical, compositional, and biological studies.

The materials exhibited complex surface topography and chemical heterogeneity that were created through the co-deposition and curing of incompatible HBFP and PEG components, where the HBFP and PEG segregated into their respective domains through differences in topology and composition, yet were covalently trapped on the molecular level through covalent bond formation. The properties of the film surfaces were observed by atomic force microscopy and static contact angle (Figure 1). It was found that submicrometer topographical features were distributed across the surface, with an overall rms roughness of 110 ± 8 nm, and the film surface had a static water contact angle of 76 ± 2°. This combination of complex nanoscopic topography and amphiphilicity presents obstacles for a settling organism, which complicates the search for an area suitable for adhesion, resulting in passive resistance to biofouling. It was expected that marine invertebrate larvae, such as barnacle cyprids, would sense surface-bound NA unfavorably and would avoid settling on those areas, resulting in an active fouling deterrence mode. However, AFM and contact angle measurements after NA conjugation gave data similar to those for the unmodified HBFP-PEG, preventing confirmation and quantification of the presence of NA on **1**.

Secondary ion mass spectrometry was employed to confirm the covalent attachment of NA to the polymer backbone. In SIMS, the primary ion plays a key role in the emission of ions, specifically the molecular ions, and for this reason C_{60} was selected as the primary ion. C_{60} is surface sensitive, generates secondary ion emission from the top 5–10 nm of a substrate, and displays higher molecular ion emission compared to atomic and small cluster projectiles.[36,37] The SIMS experiments for this study were conducted in the superstatic regime, where less than 0.1% of the surface is impacted. This limitation ensured that each time the surface was impacted by a primary ion, an unperturbed area of the surface was sampled. Superstatic measurements were conducted in the event-by-event bombardment-detection mode of operation, where a single primary ion impacted on the surface and the secondary ions were collected and analyzed prior to subsequent primary ions impacting the surface. All secondary ions detected in a single impact originated from a 10 nm radius on the surface.[38] To minimize variances between surfaces, a single HBFP-PEG film, **3a**, was obtained from a THF solution of HBFP and PEG (Scheme 1). The film was divided in half to afford two films with "identical" surfaces. These unmodified samples were analyzed by event-by-event cluster SIMS and found to have equivalent mass spectra (Figure S1). Three different regions were investigated for each sample to ensure sample consistency. In these spectra, we observed several peaks from the HBFP portion of the cross-linked network corresponding to the PFS monomer, including 191, 167, and 19 *m/z*. Larger fragments of the polymer structure were also detected, such as *m/z* 353, a fragment of the inimer-based repeat units. One film was modified by incubation in a noradrenaline/PBS solution to give **1a**, followed by sonication and washing to ensure removal of physically entrapped NA. The other film underwent the same procedure, in PBS solution, to yield **3a**. Both surfaces were analyzed after washing (Figures S2 and S3). A quantitative estimate of surface coverage of PFS was calculated,[39] and we found that the coverage of the PFS was 70% ± 5% for **3a** and 77% ± 2% for **1a**. These results supported sample consistency, given that there was a similar

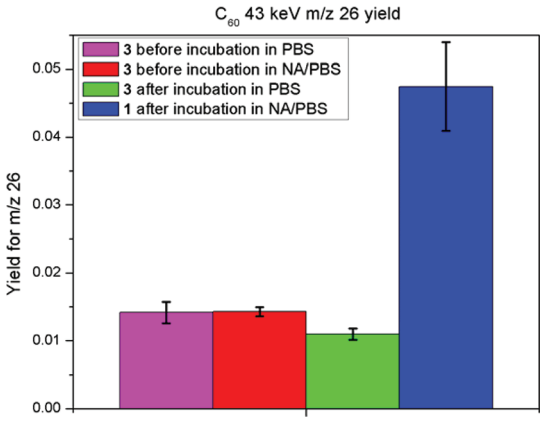

Figure 2. Yields for *m/z* 26 for 3a (before and after PBS buffer and before NA/PBS buffer) and 1a (after NA/PBS buffer).

detectable amount of PFS on either of the unmodified HBFP-PEG or modified NA-HBFP-PEG surfaces.

The existence of the covalently bound NA was substantiated by the presence of the fragment ion CN^- in the mass spectra. The intact noradrenaline was not observed due to its poor ionization in negative mode. Indirectly, NA was quantified by observing the change in yield, *Y*, defined as the number of SIs detected per projectile impact for a chosen *m/z*, for the nominal *m/z* 26 ion between the unmodified and modified samples. Although many fragment ions could potentially contribute to the *m/z* 26 peak (CN^- from the PEG chain ends, $C_2H_2^-$ from the HBFP backbone and PEG backbone), it was expected that there was an equal contribution from the polymer backbone in **3a** and **1a** because both samples were obtained from a single parent film. This assumption was verified by the consistent coverage of PFS on each surface. The 3- to 4-fold increase in *m/z* 26 yield (Figure 2) between the surfaces of **3a** and **1a** was a strong indication of NA on the surface; however, it did not indicate the selective attachment of the molecule at the labile chain ends.

To probe substitution of labile Br with NA, a calculation comparing the relative number of Br sites on **3a** and **1a** was employed (eq 1). On the surface of the films, specifically from the HBFP portion of the cross-linked network, there are finite numbers of initial Br sites, which can be viewed as both random and disperse. The initial amount of sites in **3a** was determined by calculating the ratio of Br^- to F^- yields. After tethering NA to the surface, the remaining sites were found by the same calculation for **1a**. The quotient of the ratios of the final sites (0.027 ± 0.003) to the initial sites (0.044 ± 0.002) yielded the percentage of Br sites that remained on the surface after modification (Table 1). We found that 61% of the Br sites remained after incubation with noradrenaline, indicating that NA had replaced 39% of the Br sites on the surface. The substitution of Br with NA is supported by the increase in the yield of *m/z* 26 (Figure 2). It can be shown at the

TABLE 1. Secondary Ion Yields for Br and F from Unmodified 3a and NA-Modified 1a

sample name	yield Br^-	yield F^-	Y_{Br^-}/Y_{F^-}
3a (region 1)	0.0038	0.083	0.046
3a (region 2)	0.0033	0.080	0.042
3a (region 3)	0.0041	0.093	0.044
3a (av $\pm$ SD)			0.044 ± 0.002
1a (region 1)	0.0034	0.120	0.029
1a (region 2)	0.0027	0.117	0.023
1a (region 3)	0.0035	0.122	0.029
1a (av $\pm$ SD)			0.027 ± 0.003

85% confidence level that the Br^- yield for the **3a** samples (mean value of 0.0038) are significantly different from the Br^- yields measured from sample **1a** (mean value of 0.0032), further indicating the replacement of Br.

$$\left[\frac{\frac{Y_{Br^-,NA-HBFP-PEG}}{Y_{F^-,NA-HBFP-PEG}}}{\frac{Y_{Br^-,HBFP-PEG}}{Y_{F^-,HBFP-PEG}}}\right] * 100\% = \text{percentage of unconsumed sites} \quad (1)$$

The presence of NA on the surface allowed us to test the hypothesis that the NA would act in conjunction with the complicated surface features to improve the overall antibiofouling efficiency of the system. Hemocytes (cells) of the Eastern Oyster (*C. virginica*) were used to determine if the NA molecules retained their bioactivity after covalent conjugation to the HBFP-PEG surface. Oyster hemocytes have been found to express adrenergic receptors (target receptors for NA), and the effects of NA on oyster hemocyte physiology have been well documented. In fact, hemocytes are known to undergo apoptosis (programmed cell death) upon NA stimulation.[40−43] Since oysters are a prominent fouling species and their cells express the target receptors, hemocytes make for a good model system to screen NA-conjugated polymer surfaces.[11,40] A similar strategy was employed by Gohad *et al.* to observe interactions between NA-conjugated PHEMA and PMAA polymer brushes and oyster hemocytes.[11] In that study, a cytoskeletal assay was used to confirm that covalently linked NA molecules were able to induce apoptosis in the adhering hemocytes, which was demonstrated by the loss of cell membrane integrity, abnormal accumulation of cytoskeletal elements, and finally enucleation (dislodgment of the nucleus) and membrane blebbing, hallmarks of the apoptotic progression.

A cytoskeletal assay was employed to observe the effects that unmodified HBFP-PEG and modified NA-HBFP-PEG films had on settled cell physiology. Cells adhering to unmodified HBFP-PEG surfaces **3** (Figure 3a and b) exhibited a diffused pattern of actin filaments and an absence of stress filaments. The cells had intact cell membranes and exhibited a normal morphology,

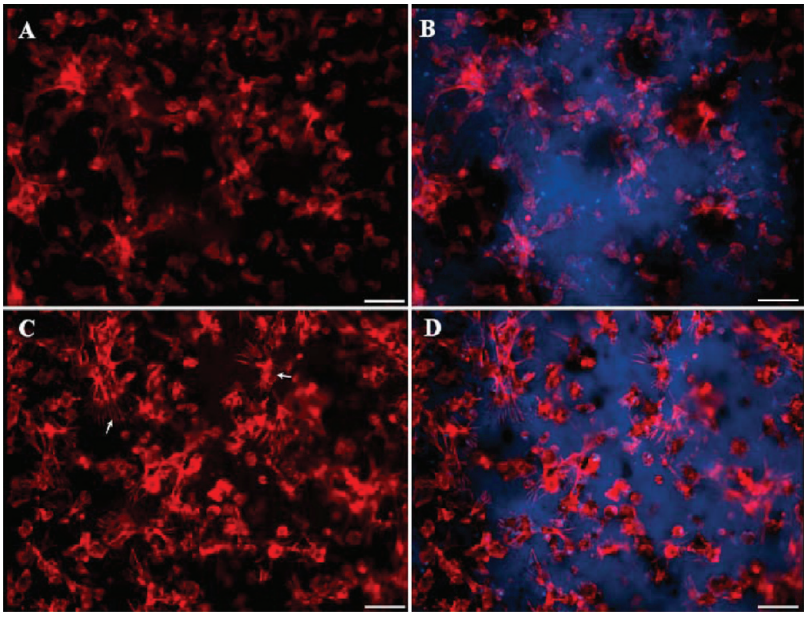

Figure 3. Cytoskeletal assay I. (A, B) Fluorescent micrograph of hemocytes interacting with unmodified HBFP-PEG surfaces stained with fluorescent phalloidin labeling F-actin (red) and DAPI labeling nuclei (blue), which display a normal morphology, intact cell membranes, and lack of actin stress filaments. (C, D) Hemocytes interacting with NA-HBFP-PEG surfaces showing an abnormal morphology with disintegrated cell membranes and the presence of actin stress filaments, hallmarks of the apoptotic cascade. Scale bar A–D: ~30 μm.

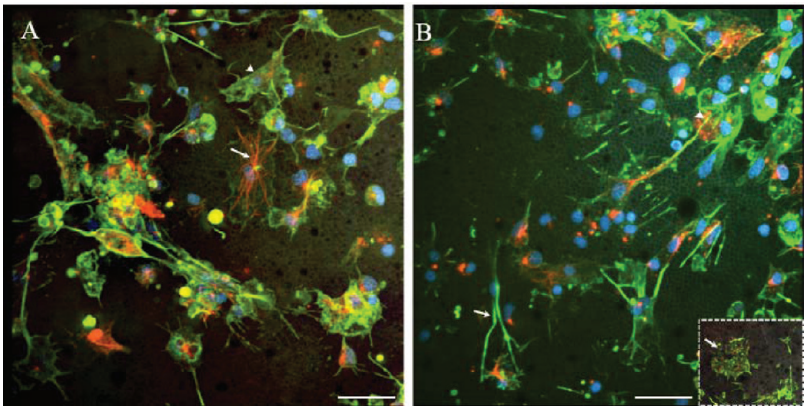

Figure 4. Cytoskeletal assay II. (A) Laser scanning confocal micrograph of hemocytes interacting with HBFP-PEG surfaces stained with phalloidin labeling F-actin (green), anti β-tubulin antibody labeling microtubules (red), and DAPI labeling nuclei (blue), which display a normal morphology, intact cell membranes (arrowhead), lack of actin stress filaments, and microtubules organized around the nucleus as the organizing center (arrow). (B) Hemocytes interacting with NA-HBFP-PEG surfaces showing disintegrated cell membranes (inset box, arrow) along with actin stress filaments and abnormal accumulation of actin (arrow). The microtubules seem to have lost the centrally organized structure and accumulate in the cytoplasm or near plasma membranes (arrowhead), indicating progression of the apoptotic cascade. Scale bars: ~20 μm.

indicating that HBFP-PEG surfaces on their own did not affect the cells adversely. In contrast, cells adhering to NA-HBFP-PEG surfaces, **1**, showed stressed actin filaments, an abnormal aggregation of actin, and disintegrated cell membranes. Extensive enucleation was also evident, indicating that cells interacting with NA-HBFP-PEG surfaces underwent apoptosis (Figure 3c and d). To confirm the effects of NA-HBFP-PEG surfaces on hemocyte physiology, the cytoskeletal assay was further modified. Gohad *et al.* had used F-actin as a marker to demonstrate cytoskeletal deterioration.[11] In this study, β-tubulin, a component of microtubules, was used in addition to F-actin. Microtubules, along with F-actin, form the cytoskeleton of cells, and any adverse effects of the cell–surface interaction can be confirmed by observing these cytoskeletal elements. Cells interacting with unmodified HBFP-PEG showed no abnormal distribution of either F-actin or β-tubulin (Figure 4a). Actin stress filaments were absent, and the microtubules were organized around the nucleus, with the nucleus serving as the organizing center, indicating that unmodified HBFP-PEG, **3**, did not adversely affect the cytoskeleton and, in turn, cell physiology. Cells interacting with NA-HBFP-PEG, **1**, not only displayed

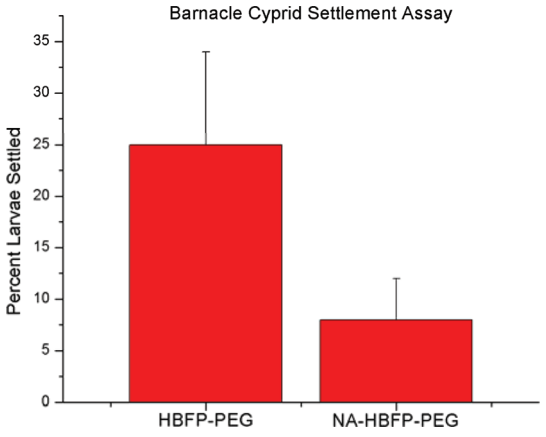

Figure 5. Cyprid settlement assay. Barnacle cyprid settlement on NA-HBFP-PEG was significantly reduced as compared to unmodified HBFP-PEG surfaces.

stressed actin filaments but also showed abnormal accumulation of microtubules with the loss of a centrally organized structure (Figure 4b).

The hemocytes being unable to internalize the receptors, considering that the NA molecules were covalently tethered to polymer surfaces, could lead to hyperstimulation of the hemocyte β-adrenergic receptors (β-AR), which could support the observed apoptosis.[11] The aberrant signaling caused by a hyperstimulated β-AR could result in the observed apoptosis in hemocytes that interacted with NA-HBFP-PEG. Gohad *et al*. postulated scenarios to explain the observed cytoskeletal deterioration in hemocytes interacting with NA-conjugated polymer surfaces.[11] The observed cytoskeletal deterioration could be a direct indicator of end stages of the apoptotic cascade, as a result of NA-induced stimulation of the hemocyte (β-AR). β-AR stimulation is known to activate L-type Ca^{2+} channels, leading to influx and overload of Ca^{2+}, which then leads to apoptosis.[11,44−46] In rat cardiomyocytes, β-AR stimulation induces microtubule disassembly *via* cAMP-mediated Ca^{2+} overload.[47] From the observed results (Figure 4b) it is possible that hyperstimulation of β-AR by polymer-tethered NA molecules could lead to microtubule disassembly in hemocytes. G-Protein coupled receptor kinase-2 (GRK2) is a signal transducer that mediates the effects of an activated (agonist bound) GPCR (G-protein coupled receptor) on the cytoskeleton by forming a complex with tubulin.[48] A hyperactivated GPCR could lead to unregulated GRK2−tubulin complex formation, causing tubulin to abnormally accumulate at the plasma membrane, which could explain the observed loss of a centrally organized structure (Figure 4b).[11] The observed actin stress filaments and disintegrated actin filaments could also be results of the apoptotic cascade. Caspases, mediators of apoptosis, cleave actin, which in turn is targeted to mitochondria and regulates the release of Ca^{2+} through inositol triphosphate and ryanodine-sensitive calcium stores. This process leads to the accumulation of Ca^{2+} in the mitochondrial matrix, forming a feedback loop that progresses the apoptotic cascade even further.[11,49]

Barnacle cyprid settlement assays showed that cyprid settlement on NA-HBFP-PEG was significantly reduced as compared to unmodified HBFP-PEG surfaces, indicating that cyprid larvae could sense the HBFP-tethered NA molecules and as a result were deterred from settling (Figure 5). When exposed to micromolar solutions of NA, barnacle cyprids are known to lose their settlement behavior and metamorphose into normal juvenile adults, which are not cemented to the substratum.[40] This behavior could perhaps be explained by the fact that barnacles express a GPCR that is almost 37% similar to the human α_2-adrenergic receptor.[50] In addition, micromolar solutions of many other adrenergic receptor ligands, such as medetomidine, clonidine, idozaxan, and phentolamine, are also known to inhibit barnacle cyprid settlement.[51,52]

It is important to discuss the observed settlement deterrence and how the cyprids are capable of sensing surface-tethered NA molecules. The fourth antennular segment of the barnacle cyprids possesses an array of sophisticated structures, the sole purpose of which is to examine the various aspects of the substratum prior to settlement.[53−55] Cyprids are known to respond favorably to surface-adsorbed molecules, as opposed to soluble ones.[56,57] While exploring the surface, the four subterminal setae and the two postaxial setae of the cyprid antennule are pressed against the substratum to possibly sense the surface-adsorbed molecules.[53,55] Since the cyprids have such a sophisticated chemosensory apparatus, it can be speculated that when HBFP-PEG-tethered NA molecules stimulate these sensors, these stimuli are, in turn, perceived as unfavorable settlement cues by the cyprids, causing deterrence of settling on such surfaces.[11] The observed reduction in larval settlement (Figure 5) further indicates that a dual mode of biofouling resistance was attainable through the addition of an active sensory deterrent to a passive antibiofouling substrate.

CONCLUSIONS

Dual-mode antibiofouling surfaces were synthesized by modifying passively antibiofouling HBFP-PEG with NA, and extensive characterization studies were performed. The co-deposition of HBFP and PEG afforded surfaces with nanoscopically resolved topography and morphology that were passively antibiofouling. Modification with the settlement deterrent NA afforded the dual-mode surface. The extent of substitution on the surface was determined by SIMS, which was quantified by the increase of *m/z* 26 and the reduction in the ratio of Br^- to F^-. The biological activity of the

system was investigated through oyster hemocyte and barnacle cyprid assays. The activity of tethered NA was confirmed by the observed cytoskeletal deterioration and apoptosis. The decoration of NA led to reduced settlement of barnacle cyprid larvae on NA-modified surfaces. The combination of passive and active modes of antibiofouling increased the overall surface performance toward the inhibition of barnacle cyprid settlement. This study provides a new strategy for combining known fouling deterrent methodologies into a single coating and will be a guide for future formulations that optimize the effective application of these materials.

MATERIALS AND METHODS

Reagents and starting materials were purchased from Sigma Aldrich and used as received unless otherwise noted. 2,3,4,5,6-Pentafluorostyrene was purchased from Apollo Scientific (UK) and filtered through a plug of neutral alumina prior to use. Monomers and polymers were characterized by ^{1}H, ^{13}C, and ^{19}F nuclear magnetic resonance spectroscopies using a Varian Inova 300 MHz spectrometer. ^{1}H and ^{13}C NMR spectra were analyzed using the solvent signal as an internal reference, and ^{19}F NMR spectra were analyzed with CF_3COOH as an external standard. IR spectra were obtained on a Shimadzu IR Prestige attenuated total reflectance Fourier-transform infrared spectrometer (ATR-FTIR). Spectra were analyzed using the IRsolution software package (Shimadzu). High-resolution mass spectrometry (HRMS) was conducted on an Applied Biosystems PE SCIEX QSTAR. Gel permeation chromatography was performed on a Waters Chromatography, Inc. (Milford, MA, USA) 1515 isocratic HPLC pump equipped with an inline degasser, a model PD2020 dual-angle (15° and 90°) light-scattering detector (Precision Detectors, Inc.), a model 2414 differential refractometer (Waters, Inc.), and four PL_{gel} polystyrene-*co*-divinylbenzene gel columns (Polymer Laboratories, Inc.) connected in series: 5 μm Guard (50 × 7.5 mm), 5 μm Mixed C (300 × 7.5 mm), 5 μm 10^4 (300 × 7.5 mm), and 5 μm 500 Å (300 × 7.5 mm) using the Breeze (version 3.30, Waters, Inc.) software. The instrument was operated at 35 °C with THF as the eluent (flow rate set to 1.00 mL/min). Polymer solutions were prepared at a known concentration (*ca.* 3 mg/mL), and an injection volume of 200 μL was used. Data collection was performed with Precision Acquire 32 acquisition program (Precision Detectors, Inc.), and analyses were carried out using Discovery32 software (Precision Detectors, Inc.) with a system calibration curve generated from plotting molecular weight as a function of retention time for a series of broad polydispersity poly(styrene) standards. Differential scanning calorimetric (DSC) studies were performed on a Mettler-Toledo DSC822^{e} (Mettler-Toledo, Inc., Columbus, OH, USA), with a heating rate of 10 °C/min. The T_g was taken as the midpoint of the inflection tangent, upon the third heating scan. Thermogravimetric analysis was performed under an Ar atmosphere using a Mettler-Toledo model TGA/DSC 1 Star^{e} system, with a heating rate of 10 °C/min. Measurements were analyzed using Mettler-Toledo Star software version 10.00c. Atomic force microscopy was performed under ambient conditions in air. The AFM instrumentation consisted of a MFP-3D-BIO AFM (Asylum Research; Santa Barbara, CA, USA) and standard silicon tips (type, OTESPA-70; L, 160 μm; normal spring constant, 50 N/m; resonance frequency, 246–282 kHz). Contact angles were measured as static contact angles using the sessile drop technique[58] with an Attension Theta optical tensiometer (Biolin Scientific). Drops were fitted with a Young–Laplace formula to calculate the static contact angle in the Theta software (Biolin Scientific). The reported values are an average of five such measurements on different regions of the same sample. Fluorescence microscopy was carried out using a Nikon Eclipse TiE microscope equipped with a CoolSnap HQ2 (Roper Scientific) monochrome CCD camera and appropriate filter sets for the fluorophores used. Confocal microscopy was performed using a Nikon Eclipse TiE microscope equipped with a Nikon C1Si spectral confocal with appropriate laser lines and filter sets for DAPI, FITC, and TRTC fluorophores.

4-[0xy(tri(ethylene glycol))]-2,3,5,6-tetrafluorostyrene (4). To a stirring solution of sodium hydride (60 wt % dispersion in mineral oil, 4.95 g, 124 mmol) in THF (400 mL) in a 1000 mL two-neck round-bottomed flask suspended in an ice bath was added tri(ethylene glycol) (41.3 mL, 309 mmol), followed by the addition of PFS (14.2 mL, 20.0 g, 103 mmol). The solution was allowed to warm to room temperature and with stirring under N_2 for 14 h. The reaction mixture was then concentrated *in vacuo*, dissolved in deionized water (300 mL), and extracted with ethyl acetate (4 × 300 mL). The organic fractions were combined, dried over anhydrous $MgSO_4$, filtered, and concentrated *in vacuo* to afford a clear, pale yellow oil. Further purification by silica gel flash chromatography using 10% MeOH in DCM as the eluent afforded **4** as a clear, colorless oil in 62% yield (20.6 g). T_{decomp}: 362 °C, 74% mass loss @ 500 °C. IR = 3600–3200, 3050–2800, 1643, 1489, 1358, 1288, 1250, 1080, 941 cm^{-1}. ^{1}H NMR (acetone-d_6, ppm): δ 6.60 (dd, J = 12 and 18 Hz, 1H, H_2C═C*H*-R), 5.96 (d, J = 18 Hz, 1H, *H*(H)C═CH-R (*trans*)), 5.65 (d, J = 12 Hz, 1H, H(*H*)C═CH-R (*cis*)), 4.38 (t, J = 5 Hz, 2H, TFS-O-C*H*$_2$-CH_2-OR), 3.78 (t, J = 5 Hz, 2H, TFS-O-CH_2-C*H*$_2$-OR′), 3.40–3.70 (m, 8H, R-O-(C*H*$_2$-C*H*$_2$-O-C*H*$_2$-C*H*$_2$-OH) ppm. ^{13}C NMR (acetone-d_6, ppm): δ 147.2, 143.7, 143.0, 140.2, 137.3, 122.5, 122.4, 122.3, 122.2, 111.0, 74.8, 73.2, 71.1, 70.8, 70.5, and 61.6 ppm. ^{19}F NMR (acetone-d_6, ppm): δ −147 (m, *ortho-F* to C═CH_2), −159 (m, *meta-F* to C═CH_2) ppm. HRMS: *m/z* calcd for $C_{14}H_{16}F_4O_4$ $[M + H]^+$ 325.10, found 325.1063.

4-[0xy(tri(ethylene glycol))bromoisopropionyl]-2,3,5,6-tetrafluorostyrene (5). To a stirring solution of triethylamine (7.70 mL, 55.5 mmol) in THF (259 mL) in a 500 mL two-neck round-bottom flask was added **4** (5.00 g, 15.4 mmol). The solution was cooled to 0 °C, and 2-bromoisopropionyl bromide (3.99 g, 18.5 mmol) was added dropwise. The solution was allowed to warm to room temperature with stirring under N_2 for 16 h. The reaction mixture was filtered, and the filtrate was then concentrated *in vacuo*, dissolved in dichloromethane (500 mL), and washed with deionized water (4 × 500 mL). The organic fraction was dried over anhydrous $MgSO_4$, filtered, and concentrated *in vacuo* to afford a clear, pale yellow oil. Further purification by silica gel flash chromatography using 30% ethyl acetate in hexanes as the eluent afforded **5** as a clear, colorless oil in 82% yield (5.81 g), which was stored at 4 °C to prevent side-reaction. T_{decomp}: 297 °C, 70% mass loss @ 500 °C. IR = 3050–2800, 2874, 2747, 1738, 1647, 1485, 1451, 1429, 1406, 1377, 1354, 1335, 1223, 1153, 1119, 1078, 1030, 968, 937, 858, 762, 677, 648 cm^{-1}. ^{1}H NMR (acetone-d_6, ppm): δ 6.60 (dd, J = 12 and 18 Hz, 1H, H_2C═C*H*-R), 5.96 (d, J = 18 Hz, 1H, *H*(H)C═CH-R (*trans*)), 5.65 (d, J = 12 Hz, 1H, H(*H*)C═CH-R (*cis*)), 4.6 (q, J = 5 Hz, 1H, R-C(*H*)(Br)CH_3), 4.5 (t, J = 5 Hz, 2H, TFS-O-C*H*$_2$-CH_2-OR), 4.3 (t, J = 5 Hz, 2H, R-CH_2-C*H*$_2$-O(O)-C-R′), 3.9 (t, J = 5 Hz, 2H, TFS-O-CH_2-C*H*$_2$-OR), 3.8–3.6 (m, 6H, R-O-C*H*$_2$-C*H*$_2$-O-C*H*$_2$-CH_2-O(O)C-R′), 1.8 (d, J = 5 Hz, 3H, R-C(H)(Br)C*H*$_3$) ppm. ^{13}C NMR ($CDCl_3$, ppm): δ 171.3, 145.7, 144.0, 141.8, 140.2, 136.4, 122.0, 121.8, 110.6, 74.1, 70.6, 70.1, 64.9, 55.6, and 30.5 ppm. ^{19}F NMR (acetone-d_6, ppm): δ −147 (m, *ortho-F* to C═CH_2), −159 (m, *meta-F* to C═CH_2) ppm. HRMS: *m/z* calcd for $C_{17}H_{19}BrF_4O_5$ $[M + H]^+$ 459.04, found 459.0439.

Hyperbranched Fluoropolymer (HBFP) (2). To a dry 50 mL Schlenk flask equipped with a stir bar was added **5** (5.00 g, 10.9 mmol, 1 equiv), PFS (6.34 g, 32.7 mmol, 3 equiv), PMDETA (3.33 g, 19.2 mmol, 2 equiv/Br), CuBr (1.57 g, 10.9 mmol, 1 equiv/Br), and anisole (100 mL). The solution was degassed *via* freeze–pump–thaw (3×), the vessel was backfilled with N_2 and then lowered into an oil bath set at 65 °C, and the reaction was

allowed to proceed for 20 h. The polymerization was quenched by opening the flask to air and submerging the flask in liquid nitrogen. Once thawed, the contents were dissolved in dichloromethane (450 mL), eluted through a plug of alumina to remove the catalyst, and concentrated *in vacuo*, and the product was isolated by precipitation into cold hexanes (3 × 1.2 L) to afford a white powder of **2** in 62% yield (7.03 g). M_w^{GPC} = 17 400 Da, M_n^{GPC} = 8600 Da, M_w/M_n = 1.72. T_g = 73 °C. T_{decomp}: 310 °C, 85% mass loss @ 500 °C. IR = 2947, 2878, 2361, 1744, 1651, 1497, 1296, 956, 864 cm^{-1}. ^1H NMR ($CDCl_3$, ppm): δ 4.6−4.0 (br, m, TFS-O-CH_2-CH_2-OR and R-CH_2-CH_2-O(O)C-R′), 4.0−3.4 (br, m, R-O-CH_2-CH_2-OR′), 3.1−1.5 (br, m, CH_2-CH(R)- backbone), δ 1.5−0.7 (br m, C-CH_3) ppm. ^{13}C NMR ($CDCl_3$, ppm): δ 176.6, 144.7, 140.7, 137.6, 122.2, 114.7, 74.3, 70.8−70.0, 68.8, 63.6, 41.7−32.1, 30.7−29.7, 24.7 ppm. ^{19}F NMR ($CDCl_3$, ppm): δ −143 (br, m, *o*-F (PFS) and *o*-F (TFS)), −157 (br, m, *p*-F (PFS) and *m*-F (TFS)), −162 (br, m, *m*-F (PFS)) ppm.

General Procedure for the Preparation of HBFP-PEG Films (3). To a scintillated vial were added **2** (0.70 g) and 1500 Da DA-PEG (0.35 g, 33 w/w % of total mass) and mixed in THF (8 mL) until homogeneous. A catalytic amount of diisopropylethylamine (100 μL) was syringed into the vial. Approximately 0.2 mL of the solution was drop cast onto precut 1 cm^2 glass microscope slides. The THF was allowed to evaporate over *ca.* 20 min, affording a pre-gel. The slides were placed in an oven purged with N_2 at 110 °C for 45 min to cure followed by submersion in a water bath overnight to leach any VOCs and release a free-standing film of **3**. θ_{H2O} = 76 ± 2°. rms roughness = 110 ± 8 nm.

General Procedure for the Preparation of Noradrenaline-Functionalized HBFP-PEG Films (1). Samples of **3** (1 × 1 cm^2) were placed individually into wells of a 12-well plate. To each well was added a solution of noradrenaline·HCl in pH 7.4 PBS (*ca.* 2 mL, 1 mg/mL). The plate was covered in Parafilm and aluminum foil and placed on an orbital shaker at 4 °C for 48 h. The solution was decanted and the coatings were rinsed with fresh, cold PBS, followed by brief sonication in cold PBS, and were stored dry under N_2 at −20 °C prior to use.

SIMS. The instrument used in these studies is a custom-built instrument equipped with a custom-built C_{60} source capable of producing C_{60}^{2+} at 43 keV total impact energy.[35,59,60] The instrument is equipped with a 1 m linear time-of-flight (ToF) and an electron emission microscope. All samples were analyzed in negative ion mode using the emitted electrons as the start for the ToF measurement. SIMS analysis was performed on a series of samples throughout the production/modification of the HBFP-PEG: two HBFP-PEG samples after hydration, unmodified HBFP-PEG after incubation in PBS, and modified NA-HBFP-PEG after incubation in NA/PBS. Two or three 200 μm radius spots were analyzed for each sample to ensure sample consistency.

Oyster Culture. Eastern Oyster (*Crasostrea Virginica*) adults were purchased from Pemaquid Oyster Company Inc. (Waldoboro, ME, USA). The oysters were maintained in a 180 gal (681 L) tank at 18 °C in artificial seawater (ASW) at 21% salinity with saturating levels of dissolved oxygen. Shellfish Diet 1800 (Reed Mariculture Inc.) was used to feed the animals. Hemocytes (immune cells) were obtained by notching the oyster shell with a cement saw and extracting the hemolymph from the adductor muscle with a 22-guage needle affixed to a disposable syringe.[61] Depending on the size and weight of the oyster, 1−2 mL of hemolymph was extracted.

Cytoskeletal Assay I. Cytoskeletal assay I was performed as described by Gohad *et al.*[11] Briefly, 500 μL of hemolymph was aliquated onto unmodified HBFP-PEG and NA-HBFP-PEG substrates, and hemocytes were allowed to settle on surfaces for 60 min. Cells were then fixed with 4% formaldehyde freshly prepared from paraformaldehyde, made up in phosphate buffer saline (PBS) for 40 min. Surfaces were rinsed twice for 5 min each on an orbital shaker to remove any unreacted formaldehyde. For staining with fluorescent phalloidin labeling F-actin, cells were permeabalized by incubating in 0.1% Triton-X100 in PBS for 5 min. Surfaces were then washed twice for 5 min each, then incubated in a 50 μM solution of TRITC-Phalloidin (Sigma) for 45 min, and washed twice to remove excess phalloidin. Hemocytes were then counterstained with DAPI, labeling nuclei, and fluorescence microscopy was carried out.

Cytoskeletal Assay II. Hemocytes incubated on HBFP-PEG and NA-HBFP-PEG were fixed and permeabalized as described above. Cells on surfaces were then blocked using a 4% solution of bovine serum albumin (Sigma) made up in PBS for 40 min. Then, the surfaces were incubated in a 1:500 dilution of anti-beta tubulin antibody (Developmental Studies Hybridoma Bank) overnight at 4 °C. The surfaces were then washed twice for 5 min each and incubated with a 1:1000 dilution of Alexa-Fluor-555 fluorescent secondary antibody (Life Technologies) for 1 h. Surfaces were washed twice for 5 min each and incubated with a 50 μM solution of FITC-Phalloidin (Sigma) labeling F-actin for 45 min, the samples were counterstained with DAPI, labeling nuclei, and confocal microscopy was carried out.

Control samples for cytoskeletal assay II (hemocytes on HBFP-PEG and NA-HBFP-PEG) were labeled only with the fluorescent secondary antibody to rule out any nonspecific interactions between the secondary antibody and samples. Control samples did not show any nonspecific labeling with the fluorescent secondary antibody.

Unstained HBFP-PEG and NA-HBFP-PEG with hemocytes were also used as autofluorescence controls and inspected under the microscope using the same excitation and emission filter sets and imaging modalities (wide field fluorescence and confocal microscopy) for DAPI, FITC, and TRITC fluorophores. Unstained samples were not found to be autofluorescent in either of the imaging modalities.

Cyprid Settlement Assays. Cyprid (settlement stage) larvae of the striped barnacle *Balanus amphitrite* were obtained from Dr. Dan Rittschof's laboratory at Duke University Marine Laboratory and were shipped and handled as described previously.[28] HBFP-PEG and NA-HBFP-PEG surfaces were placed in 24-well plates (Kimtec), filled with ASW, washed several times, and allowed to equilibrate with ASW for 10 min. The 1 × 1 cm^2 samples covered the majority of the surface area of the well bottom. Approximately 16 to 20 cyprids were added to each well in ASW, after which the plates were covered with aluminum foil and placed in a humid chamber at room temperature for 48 h. At the end of the incubation period, number of settled cyprids was counted for each well using the Nikon-AZ100 macroscope. The percentage of total larvae settled was calculated for NA-conjugated and control surfaces and subjected to a one-way ANOVA with the significance cutoff set to $p \leq 0.05$.

Conflict of Interest: The authors declare no competing financial interest.

Acknowledgment. Financial support was provided by the Office of Naval Research under Grant Numbers N00014-10-1-0527 (K.L.W.) and N00014-08-1-0157 (A.S.M. and N.V.G.), the National Science Foundation, Grant No. CHE-0750377 (E.A.S.), and the W. T. Doherty-Welch Chair in Chemistry, Grant No. A-0001 (K.L.W.). We also thank the Texas A&M University Laboratory for Biological Mass Spectrometry for small-molecule mass spectral analysis. The anti-beta tubulin monoclonal antibody developed by M. Klymkowsky was obtained from the Developmental Studies Hybridoma Bank developed under the auspices of the NICHD and maintained by the University of Iowa, Department of Biology, Iowa City, IA.

Supporting Information Available: Additional SIMS spectra. This material is available free of charge *via* the Internet at http://pubs.acs.org.

REFERENCES AND NOTES

1. Schultz, M. P. Effects of Coating Roughness and Biofouling on Ship Resistance and Powering. *Biofouling* **2007**, *23*, 331–341.
2. Schultz, M. P.; Bendick, J. A.; Holm, E. R.; Hertel, W. M. Economic Impact of Biofouling on a Naval Surface Ship. *Biofouling* **2011**, *27*, 87–98.
3. http://www.onr.navy.mil/media-center/fact-sheets/biofouling-prevention.aspx (accessed on August 2011).

4. Yebra, D. M.; Kiil, S.; Dam-Johansen, K. Antifouling Technology—Past, Present and Future Steps Towards Efficient and Environmentally Friendly Antifouling Coatings. *Prog. Org. Coat.* **2004**, *50*, 75–104.
5. http://www.copperantifouling.com (accessed in August 2011).
6. Zhou, J.; Zhu, X.-S.; Cai, Z.-H. Tributyltin Toxicity in Abalone (*Haliotis diversicolor supertexta*) Assessed by Antioxidant Enzyme Activity, Metabolic Response, and Histopathology. *J. Hazard. Mater.* **2010**, *183*, 428–433.
7. Srinivasan, M.; Swain, G. W. Managing the Use of Copper-Based Antifouling Paints. *Environ. Manage.* **2007**, *39*, 423–441.
8. Walters, L. J.; Miron, G.; Bourget, E. Endoscopic Observations of Invertebrate Larval Substratum Exploration and Settlement. *Mar. Ecol.: Prog. Ser.* **1999**, *182*, 95–108.
9. Berglin, M.; Wynne, K. J.; Gatenholm, P. Fouling-Release Coatings Prepared from α,ω-Dihydroxypoly(Dimethylsiloxane) Cross-Linked with (Heptadecafluoro-1,1,2,2-Tetrahydrodecyl-)Triethoxysilane. *J. Colloid Interface Sci.* **2003**, *257*, 383–391.
10. Majumdar, P.; Crowley, E.; Htet, M.; Stafslien, S. J.; Daniels, J.; VanderWal, L.; Chisholm, B. J. Combinatorial Materials Research Applied to the Development of New Surface Coatings XV: An Investigation of Polysiloxane Anti-Fouling/Fouling-Release Coatings Containing Tethered Quaternary Ammonium Salt Groups. *ACS Comb. Sci.* **2011**, *13*, 298–309.
11. Gohad, N. V.; Shah, N. M.; Metters, A. T.; Mount, A. S. Noradrenaline Deters Marine Invertebrate Biofouling When Covalently Bound in Polymeric Coatings. *J. Exp. Mar. Biol. Ecol.* **2010**, *394*, 63–73.
12. Bartels, J. W.; Cheng, C.; Powell, K. T.; Xu, J.; Wooley, K. L. Hyperbranched Fluoropolymers and Their Hybridization into Complex Amphiphilic Crosslinked Copolymer Networks. *Macromol. Chem. Phys.* **2007**, *208*, 1676–1687.
13. Xu, J.; Bartels, J. W.; Bohnsack, D. A.; Tseng, T.-C.; Mackay, M. E.; Wooley, K. L. Hierarchical Inorganic—Organic Nanocomposites Possessing Amphiphilic and Morphological Complexities: Influence of Nanofiller Dispersion on Mechanical Performance. *Adv. Funct. Mater.* **2008**, *18*, 2733–2744.
14. Xu, J.; Bohnsack, D. A.; Mackay, M. E.; Wooley, K. L. Unusual Mechanical Performance of Amphiphilic Crosslinked Polymer Networks. *J. Am. Chem. Soc.* **2006**, *129*, 506–507.
15. Chen, Y.; Liu, D.; Deng, Q.; He, X.; Wang, X. Atom Transfer Radical Polymerization Directly from Poly(vinylidene fluoride): Surface and Antifouling Properties. *J. Polym. Sci., Part A: Polym. Chem.* **2006**, *44*, 3434–3443.
16. Woodward, I.; Schofield, C. E.; Roucoules, V.; Badyal, J. P. S Super-Hydrophobic Surfaces Produced by Plasma Fluorination of Polybutadiene Films. *Langmuir* **2003**, *19*, 3432–3438.
17. Yarbrough, J. C.; Rolland, J. P.; DeSimone, J. M.; Callow, M. E.; Finlay, J. A.; Callow, J. A. Contact Angle Analysis, Surface Dynamics, and Biofouling Characteristics of Cross-Linkable, Random Perfluoropolyether-Based Graft Terpolymers. *Macromolecules* **2006**, *39*, 2521–2528.
18. Krishnan, S.; Wang, N.; Ober, C. K.; Finlay, J. A.; Callow, M. E.; Callow, J. A.; Hexemer, A.; Sohn, K. E.; Kramer, E. J.; Fischer, D. A. Comparison of the Fouling Release Properties of Hydrophobic Fluorinated and Hydrophilic Pegylated Block Copolymer Surfaces: Attachment Strength of the Diatom *Navicula* and the Green Alga *Ulva*. *Biomacromolecules* **2006**, *7*, 1449–1462.
19. Ostuni, E.; Chapman, R. G.; Liang, M. N.; Meluleni, G.; Pier, G.; Ingber, D. E.; Whitesides, G. M. Self-Assembled Monolayers That Resist the Adsorption of Proteins and the Adhesion of Bacterial and Mammalian Cells. *Langmuir* **2001**, *17*, 6336–6343.
20. Sundaram, H. S.; Cho, Y.; Dimitriou, M. D.; Weinman, C. J.; Finlay, J. A.; Cone, G.; Callow, M. E.; Callow, J. A.; Kramer, E. J.; Ober, C. K. Fluorine-Free Mixed Amphiphilic Polymers Based on PDMS and PEG Side Chains for Fouling Release Applications. *Biofouling* **2011**, *27*, 589–601.
21. Gudipati, C. S.; Finlay, J. A.; Callow, J. A.; Callow, M. E.; Wooley, K. L. The Antifouling and Fouling-Release Perfomance of Hyperbranched Fluoropolymer (HBFP)-Poly(Ethylene Glycol) (PEG) Composite Coatings Evaluated by Adsorption of Biomacromolecules and the Green Fouling Alga *Ulva*. *Langmuir* **2005**, *21*, 3044–3053.
22. Gudipati, C. S.; Greenlief, M.; Johnson, J. A.; Prayongpan, P.; Wooley, K. L. Hyperbranched Fluoropolymer and Linear Poly(Ethylene Glycol) Based Amphiphilic Crosslinked Networks as Efficient Antifouling Coatings: An Insight into the Surface Compositions, Topographies, and Morphologies. *J. Polym. Sci., Part A: Polym. Chem.* **2004**, *42*, 6193–6208.
23. Powell, K. T.; Cheng, C.; Wooley, K. L.; Singh, A.; Urban, M. Complex Amphiphilic Networks Derived from Diamine-Terminated Poly(Ethylene Glycol) and Benzylic Chloride-Functionalized Hyperbranched Fluoropolymers. *J. Polym. Sci., Part A: Polym. Chem.* **2006**, *44*, 4782–4794.
24. Coon, S. L.; Bonar, D. B. Induction of Settlement and Metamorphosis of the Pacific Oyster, *Crassostrea gigas* (Thungberg), by L-Dopa and Catecholamines. *J. Exp. Mar. Biol. Ecol.* **1985**, *94*, 211–221.
25. Coon, S. L.; Bonar, D. B. Pharmacological Evidence That α_1-Adrenoceptors Mediate Metamorphosis of the Pacific Oyster, *Crassostrea gigas*. *Neuroscience* **1987**, *23*, 1169–1174.
26. Coon, S. L.; Bonar, D. B.; Weiner, R. M. Chemical Production of Cultchless Oyster Spat Using Epinephrine and Norepinephrine. *Aquaculture* **1986**, *58*, 255–262.
27. Dahlström, M.; Lindgren, F.; Berntsson, K.; Sjögren, M.; Mårtensson, L. G. E.; Jonsson, P. R.; Elwing, H. Evidence for Different Pharmacological Targets for Imidazoline Compounds Inhibiting Settlement of the Barnacle *Balanus improvisus*. *J. Exp. Zool.* **2005**, *303A*, 551–562.
28. Gohad, N. V.; Dickinson, G. H.; Orihuela, B.; Rittschof, D.; Mount, A. S. Visualization of Putative Ion-Transporting Epithelia in *Amphibalanus amphitrite* Using Correlative Microscopy: Potential Function in Osmoregulation and Biomineralization. *J. Exp. Mar. Biol. Ecol.* **2009**, *380*, 88–98.
29. Dahlström, M.; Mårtensson, L. G. E.; Jonsson, P. R.; Arnebrant, T.; Elwing, H. Surface Active Adrenoreceptor Compounds Prevent the Settlement of Cyrpid Larvae of *Balanus improvisus*. *Biofouling* **2000**, *16*, 191–203.
30. Powell, K. T.; Cheng, C.; Wooley, K. L. Complex Amphiphilic Hyperbranched Fluoropolymers by Atom Transfer Radical Self-Condensing Vinyl (Co)Polymerization. *Macromolecules* **2007**, *40*, 4509–4515.
31. Benninghoven, A. Surface-Analysis by Secondary-Ion Mass-Spectrometry (SIMS). *Surf. Sci.* **1994**, *300*, 246–260.
32. Mahoney, C. M. Cluster Secondary Ion Mass Spectrometry of Polymers and Related Materials. *Mass Spectrom. Rev.* **2010**, *29*, 247–293.
33. Pinnick, V. T.; Verkhoturov, S. V.; Kaledin, L.; Bisrat, Y.; Schweikert, E. A. Molecular Identification of Individual Nano-Objects. *Anal. Chem.* **2009**, *81*, 7527–7531.
34. Touboul, D.; Brunelle, A.; Halgand, F.; De La Porte, S.; Laprevote, O. Lipid Imaging by Gold Cluster Time-of-Flight Secondary Ion Mass Spectrometry: Application to Duchenne Muscular Dystrophy. *J. Lipid Res.* **2005**, *46*, 1388–1395.
35. Fernandez-Lima, F. A.; Eller, M. J.; Verkhoturov, S. V.; Della-Negra, S.; Schweikert, E. A. Photon, Electron, and Secondary Ion Emission from Single C-60 keV Impacts. *J. Phys. Chem. Lett.* **2010**, *1*, 3510–3513.
36. Weibel, D.; Wong, S.; Lockyer, N.; Blenkinsopp, P.; Hill, R.; Vickerman, J. C. A C-60 Primary Ion Beam System for Time of Flight Secondary Ion Mass Spectrometry: Its Development and Secondary Ion Yield Characteristics. *Anal. Chem.* **2003**, *75*, 1754–1764.
37. Fletcher, J. S.; Conlan, X. A.; Jones, E. A.; Biddulph, G.; Lockyer, N. P.; Vickerman, J. C. TOF-SIMS Analysis Using C-60-Effect of Impact Energy on Yield and Damage. *Anal. Chem.* **2006**, *78*, 1827–1831.
38. Li, Z.; Verkhoturov, S. V.; Schweikert, E. A. Nanovolume Analysis with Secondary Ion Mass Spectrometry Using Massive Projectiles. *Anal. Chem.* **2006**, *78*, 7410–7416.
39. Chen, L. J.; Shah, S. S.; Silangcruz, J.; Eller, M. J.; Verkhoturov, S. V.; Revzin, A.; Schweikert, E. A. Characterization and

Quantification of Nanoparticle-Antibody Conjugates on Cells Using C-60 TOF SIMS in the Event-by-Event Bombardment/Detection Mode. *Int. J. Mass Spectrom.* **2011**, *303*, 97–102.
40. Gohad, N. V. Development of a Novel Fouling Deterrence Strategy by Understanding the Effect of Noradrenaline on the Cells of Eastern Oyster, *Crassostrea virginica* and Cypris Larvae of the Striped Barnacle, *Balanus amphitrite*. Clemson Univ, 2008.
41. Lacoste, A.; De Cian, M.-C.; Cueff, A.; Poulet, S. A. Noradrenaline and A-Adrenergic Signaling Induce the Hsp70 Gene Promoter in Mollusc Immune Cells. *J. Cell Sci.* **2001**, *114*, 3557–3564.
42. Lacoste, A.; Malham, S. K.; Cueff, A.; Jalabert, F.; Gelebart, F.; Poulet, S. A. Evidence for a Form of Adrenergic Response to Stress in the Mollusc *Crassostrea gigas*. *J. Exp. Biol.* **2001**, *204*, 1247–1255.
43. Lacoste, A.; Malham, S. K.; Cueff, A.; Poulet, S. A. Noradrenaline Modulates Oyster Hemocyte Phagocytosis Via a Beta-Adrenergic Receptor−Camp Signaling Pathway. *Gen. Comp. Endrocrinol.* **2001**, *122*, 252–259.
44. Lohse, M. J.; Engelhardt, S.; Eschenhagen, T. What Is the Role of B-Adrenergic Signaling in Heart Failure?. *Circ. Res.* **2003**, *93*, 896–906.
45. Xiao, R.-P. B-Adrenergic Signaling in the Heart: Dual Coupling of the B2-Adrenergic Receptor to Gs and Gi Proteins. *Sci. STKE* **2001**, *104*, re15.
46. Zhong, J.; Hume, J. R.; Keef, K. D. B-Adrenergic Receptor Stimulation of L-Type Ca^{2+} Channels in Rabbit Portal Vein Myocytes Involves Both as and by G Protein Subunits. *J. Physiol.* **2001**, *531*, 105–115.
47. Hori, M.; Sato, H.; Kitakaze, M.; Iwai, K.; Takeda, H.; Inoue, M.; Kamada, T. B-Adrenergic Stimulation Disassembles Microtubules in Neonatal Rat Cultured Cardiomyocytes through Intracellular Ca2′ Overload. *Circ. Res.* **1994**, *75*, 324–334.
48. Pitcher, J. A.; Hall, R. A.; Daaka, Y.; Zhang, J.; Ferguson, S. S. G.; Hester, S.; Miller, S.; Caron, M. G.; Lefkowitz, R. J.; Barak, L. S. The G Protein-Receptor Kinase 2 Is a Microtubule-Associated Protein Kinase That Phosphorylates Tubulin. *J. Biol. Chem.* **1998**, *273*, 12316–12324.
49. Gourlay, C. W.; Ayscough, K. R. The Actin Cytoskeleton: A Key Regulator of Apoptosis and Ageing?. *Nat. Rev. Mol. Cell. Biol.* **2005**, *6*, 583–589.
50. Isoai, A.; Kawahara, H.; Okazaki, Y.-I.; Shizuri, Y. Molecular Cloning of a New Member of the Putative G Protein-Coupled Receptor Gene from Barnacle *Balanus amphitrite*. *Gene* **1996**, *175*, 95–100.
51. Dahlström, M. Pharmacological Agents Targeted against Barnacles As Lead Molecules in New Antifouling Technologies. Goteborg University, 2004.
52. Dahms, H.-U.; Qian, P.-E. Adrenoceptor Compounds Prevent the Settlement of Marine Invertebrate Larvae: *Balanus amphitrite* (Cirripedia), *Bugula neritina* (Bryozoa) and *Hydroides elegans* (Polychaeta). *Biofouling* **2004**, *20*, 313–321.
53. Bielecki, J.; Chan, B. K. K.; Hoeg, J. T.; Sari, A. Antennular Sensory Organs in Cyprids of Balanomorphan Cirripedes: Standardizing Terminology Using *Megabalanus rosa*. *Biofouling* **2009**, *25*, 203–214.
54. Lagersson, N. C.; Garm, A.; Hoeg, J. T. Notes on the Ultrastructure of the Setae on the Fourth Antennulary Segment of the *Balanus amphitrite* Cyprid (Crustacea: Cirripedia: Thoracica). *J. Mar. Biol. Assoc. U.K.* **2003**, *83*, 361–365.
55. Maruzzo, D.; Conlan, S.; Aldred, N.; Clare, A. S.; Hoeg, J. T. Video Observation of Surface Exploration in Cyprids of Balanus Amphitrite: The Movements of Antennular Sensory Setae. *Biofouling* **2011**, *27*, 225–239.
56. Crisp, D. J. Surface Chemistry, a Factor in the Settlement of Marine Invertebrate Larvae. *Bot. Gothburgensia* **1965**, *3*, 51–65.
57. Crisp, D. J.; Meadows, P. S. Adsorbed Layers: The Stimulus to Settlement in Barnacles. *Proc. R. Soc. London B* **1963**, *158*, 364–387.
58. Neumann, A. W.; Good, R. J. Techniques of Measuring Contact Angles [in Surface Studies]. *J. Surf. Colloid Sci.* **1979**, *11*, 31–91.
59. Eller, M. J.; Verkhoturov, S. V.; Della-Negra, S.; Rickman, R. D.; Schweikert, E. A. Real-Time Localization of Single C-60 Impacts with Correlated Secondary Ion Detection. *Surf. Interface Anal.* **2011**, *43*, 484–487.
60. Verkhoturov, S. V.; Eller, M. J.; Rickman, R. D.; Della-Negra, S.; Schweikert, E. A. Single Impacts of C-60 on Solids: Emission of Electrons, Ions and Prospects for Surface Mapping. *J. Phys. Chem. C* **2010**, *114*, 5637–5644.
61. Mount, A. S.; Wheeler, A. P.; Paradkar, R. P.; Snider, D. Hemocyte-Mediated Shell Mineralization in the Eastern Oyster. *Science* **2004**, *304*, 297–300.